Microstructure and interface evolution of PtMn bottom spin-filter spin valves induced by stress and unidirectional field annealing

2005 J. Phys.: Condens. Matter 17 4073

(http://iopscience.iop.org/0953-8984/17/26/007)

INSTITUTE OF PHYSICS PUBLISHING JOURNAL OF PHYSICS: CONDENSED MATTER

J. Phys.: Condens. Matter **17** (2005) 4073–4081 doi:10.1088/0953-8984/17/26/007

Microstructure and interface evolution of PtMn bottom spin-filter spin valves induced by stress and unidirectional field annealing

R Mustafa Öksüzoglu[1,4], Ian MacLaren[2,5], Christoph Schug[3] and Hartmut Fuess[2]

[1] Department of Physics, Faculty of Science and Art, University of Selcuk, Campus, 42031 Konya, Turkey
[2] Institute for Materials Science, Darmstadt University of Technology, Petersenstrasse 23, D-64287 Darmstadt, Germany
[3] Naomi Technologies AG, Hechtsheimerstraße 2, D-55131 Mainz, Germany

E-mail: rmoksuzoglu@selcuk.edu.tr

Received 4 December 2004, in final form 10 May 2005
Published 17 June 2005
Online at stacks.iop.org/JPhysCM/17/4073

Abstract

The microstructure evolution in PtMn-based bottom spin-filter spin valves was investigated to clarify the alteration of the sensor performance caused by different annealing treatments during manufacturing. Neither unidirectional field annealing (UDA) nor stress annealing (SA) for 38 h, which simulates the final quality test of the finished read-write head, have any significant influence on the ⟨111⟩ texture of the sensor stack. UDA causes the appearance of domain boundaries in the PtMn layer as a consequence of the fcc–fct transformation together with some disturbance in the functional layers of the sensor, neither of which affect the giant magneto-resistive performance. The SA treatment causes an inter-diffusion in the NiFeCr/NiFe seed layers, some grain growth in PtMn, more serious disturbance of the functional layers, and complete amorphization of the Ta cap layer. In comparison to other studies of spin valves, the intermixing of seed layers in the present study does not appear to influence the PtMn/CoFe interface. The alteration of the sensor performance seems to be mainly caused by the inter-diffusion of the functional layers.

1. Introduction

Spin valves with synthetic ferrimagnets, the so-called spin-filter spin valves (SFSVs), have been widely utilized in recording heads and magnetoresistive random access memory applications. In particular, SFSVs with anti-ferromagnetic PtMn films have gained increasing attention

[4] Author to whom any correspondence should be addressed.
[5] Present address: Department of Physics and Astronomy, University of Glasgow, Glasgow G12 8QQ, UK.

because of their high blocking temperature [1–3] and high exchange interaction field (H_{ex}), which results in small sensor dimensions and a high reliability for higher recording densities [4]. However, the inevitable post-deposition annealing to induce the fcc–fct phase transformation in PtMn films, additional heat treatments during manufacturing, and the operating temperature, make the thermal stability of the giant magneto-resistive (GMR) sensors extremely important. Consequently, the influences of temperature, time and external magnetic field on post-deposition annealing have been extensively investigated in the last decade (e.g. [5–7]).

In our previous study, the process conditions and their influence on the sensor performance were investigated using a so-called stress annealing (SA) subsequent to the unidirectional annealing (UDA) treatment [7]. The SA treatment simulates the annealing steps after UDA and can be considered as a final outgoing quality test of the sensor's thermal stability. A UDA time-dependent alteration of sensor GMR performance after SA treatment was found in PtMn-based bottom SFSVs with a NiFeCr/NiFe seed layer [7].

In the present study, our purpose was to clarify the evolution of microstructure and interface roughnesses in SFSV sensors before and after annealing treatments by means of high-resolution transmission electron microscopy (HRTEM), in-plane x-ray diffraction (in-plane XRD) and x-ray reflectivity (XRR).

2. Experimental details

The PtMn-based SFSV sensors were prepared onto Si/1000 nm thermal SiO_2 substrates, coated with a 3 nm amorphous Al_2O_3 layer, by a DC magnetron sputtering system using Ar gas at pressures of 2–3 mTorr, without substrate heating. The target materials had a purity of 99.9%. For the sensor structures studied here a system of anti-parallel pinned (APP) CoFe/Ru/CoFe layers with a PtMn pinning layer was used, resulting in the following layer sequence: $Si/SiO_2/Al_2O_3$/NiFeCr/NiFe/PtMn(17 nm)/CoFe(2 nm)/Ru(8 nm)/CoFe(2 nm)/Cu(2 nm)/CoFe(1 nm)/NiFe(1 nm)/Cu-oxide/Ta(4 nm). The APP layers are separated by the thin Cu layer from the CoFe/NiFe layers, the so-called free layers. The purpose of the NiFeCr/NiFe seed layer is to induce a desired ⟨111⟩ texture of the subsequent—mostly cubic—metallic films. The uniaxial in-plane anisotropy of the CoFe/NiFe free layer was caused by a magnetic field of 2 mT during deposition. The SFSV sensors as-deposited, after 5 and 6 h UDA, and 6 h UDA + 38 h SA treatments, were chosen for the microstructural investigations. In addition to that, for in-plane XRD investigations, layers of SFSV were deposited successively on the same substrates and protected with a Ta layer, resulting in the following samples: NiFeCr/NiFe/Ta, NiFeCr/NiFe/PtMn/Ta, NiFeCr/NiFe/PtMn/CoFe/Ta, NiFeCr/NiFe/PtMn/CoFe/Ru/Ta, NiFeCr/NiFe/PtMn/CoFe/Ru/CoFe/Ta, NiFeCr/NiFe/PtMn/CoFe/Ru/CoFe/Cu/Ta, NiFeCr/NiFe/ PtMn/CoFe/Ru/CoFe/Cu/CoFe/Ta, NiFeCr/NiFe/PtMn/CoFe/Ru/CoFe/Cu/CoFe/NiFe/Ta, NiFeCr/NiFe/PtMn/CoFe/Ru/CoFe/Cu/CoFe/NiFe/Cu-oxide/Ta.

UDA was performed at 265 °C in an external magnetic field of 13 kOe in an inert gas (N_2) atmosphere for different annealing times. SA was carried out under a vacuum better than 1×10^{-5} Torr in one run by using the following temperature profile: (1) 200 °C for 1 h (2) 280 °C from 1 to 38 h.

Specular XRR measurements were carried out using a Bede D1 diffractometer, equipped with a sealed tube Cu source and a parabolic multilayer primary optic to generate a monochromatic (Cu Kα, $\lambda = 1.54$ Å) and collimated (divergence ∼0.02°) beam. With a fixed slit assembly, the system records specular XRR curves with a dynamic intensity range of roughly seven orders of magnitude. The experimental specular XRR data were analysed using the commercial Bede REFS software [8]. Using a genetic algorithm, it obtains the best-fit

simulation to the experimental data for multilayer structures by automatically adjusting the following parameters: the layer thicknesses t_i, RMS roughness values σ_i and mass densities ρ_i. To obtain adequate fits of the low-intensity data encountered in the high-θ region of the XRR curves, an absolute log weighting of the intensity difference between experimental and theoretical data was chosen for this work. Since the diffuse scattering contribution was negligible ($\sim$0.90 cps compared to measured incident intensity of $\sim 1.5 \times 10^7$ cps), it has not been subtracted from the measured specular reflectivity.

Cross-section samples of the thin films for the HRTEM investigation were prepared using the sandwich technique. The samples were cut into two pieces and glued face-to-face using two-component epoxy resin (Measurements Group, M-bond 610). Thin slices of about 0.5 mm were cut from the sample using a wire saw assisted by a dispersion of ultra-fine silicon carbide in water. Further thinning was carried out by mechanical polishing (diamond lapping-film, Casalin Company) and finally by Ar^+ ion milling (Rapid etching system 010, Baltec, Liechtenstein; parameters 4.5 kV, 1.0–1.5 mA at incident angles of 4°–12° for 2–6 h). The thinned samples were examined in a JEOL 3010UHR transmission electron microscope operated at 300 kV equipped with a Gatan image filter (GIF) (Gatan Inc., Pleasanton, CA). The HRTEM images were recorded using the GIF-CCD camera, and zero-loss filtering was used in some cases to improve image quality. The resulting digital images were analysed using the Gatan Digital Micrograph software (Gatan Inc., Pleasanton, CA).

3. Results and discussion

SA up to 12 h causes a reduction of the GMR to a value which then remains almost unchanged for longer (SA) times up to 38 h, although the H_{ex} increases by $\sim$8% after 2 h SA and then remains unchanged for the sensors with 5 and 6 h UDA treatments as reported in our previous work [7]. The overall reduction of the GMR value varies from 0.025% to 0.04% and becomes more pronounced with increasing UDA duration prior to SA, while the increase of the sensor resistance $R(0)$ becomes smaller [7].

In-plane XRD patterns recorded from the successively deposited sensor layer sequences are shown in figure 1 to illustrate the microstructure of each layer of the as-deposited SFSV. The following diffraction peaks can be unambiguously attributed to the individual functional layers: fcc NiFeCr/NiFe (220), fcc PtMn (220), hexagonal Ru (100), (102), (110) and (200), fcc CoFe/Cu/CoFe/NiFe (220) and nano-crystalline, most likely bcc Ta (110). The broad peak at $\sim$38° labelled as 'nano-Ta' in figure 1 come from the Ta cap layer of the NiFeCr/NiFe bilayer, since all samples were protected with a Ta cap layer (see experimental details). Due to the in-plane diffraction geometry applied here, the fcc (220) peak of the NiFeCr/NiFe seed layer and consequently that of PtMn as well as of the CoFe/Cu/CoFe/NiFe layers appears with the largest intensity for the as-deposited state. This is consistent with a sharp ⟨111⟩ out-of-plane texture of the PtMn layer induced by the seed layer. Apart from the strongly distorted hexagonal Ru layer all functional layers possess the same ⟨111⟩ texture (figure 1). In comparison a sharp ⟨111⟩ out-of-plane texture was also derived from in-plane diffractograms of an SFSV full stack after 6 h UDA treatment accompanied by a partial oxidation of the Ta cap layer [7]. Consequently, we conclude that UDA of the SFSV only causes a structural change in the PtMn ($L1_0$ ordering transition from fcc–fct)—while retaining the ⟨111⟩ texture—and a partial oxidation of the Ta cap layer.

In order to study the evolution of individual functional film thicknesses and interface roughness values upon annealing, XRR was performed with an SFSV full stack as-deposited, after 6 h UDA and after 6 h UDA + 38 h SA, respectively.

Figure 2 shows the experimental XRR data and their corresponding best-fit curves. Distinct changes of the XRR patterns can be observed for incident angles θ smaller than about 1.5°,

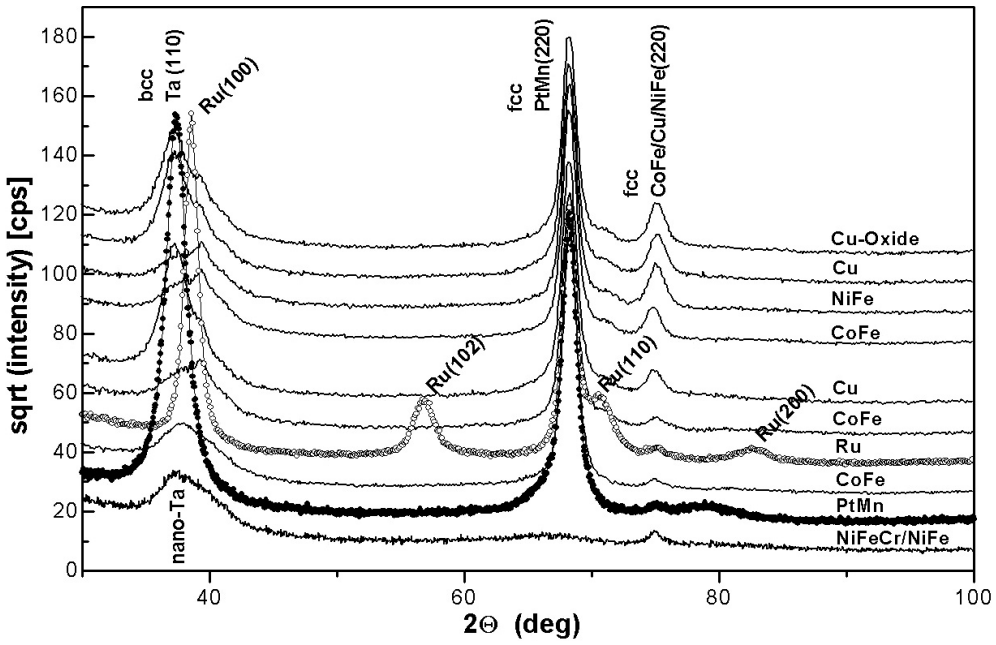

Figure 1. In-plane XRD patterns of successively SFSV layer sequence. The data are vertically shifted for clarity. The labelling NiFeCr/NiFe means XRD pattern for NiFeCr/NiFe/Ta sample and the PtMn for NiFeCr/NiFe/PtMn/Ta and the CoFe for NiFeCr/NiFe/PtMn/CoFe/Ta, etc.

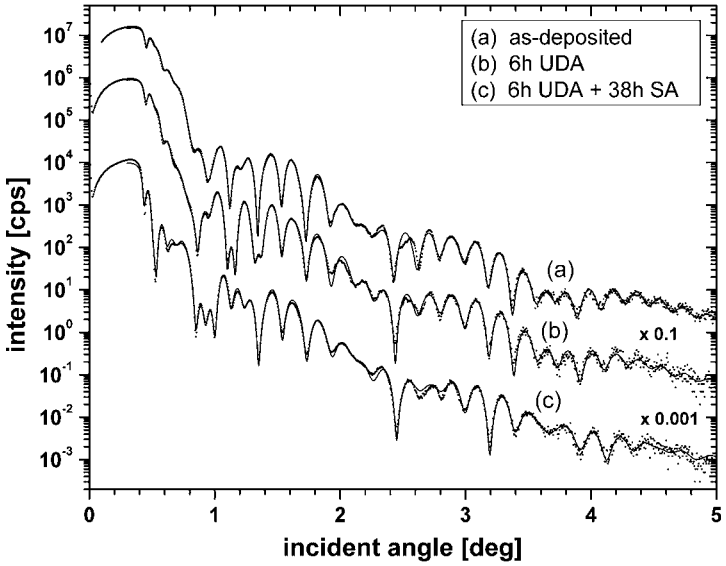

Figure 2. Experimental XRR data (dots) and corresponding best-fit simulations (straight lines) of (a) as-deposited, (b) 6 h UDA and (c) 6 h UDA + 38 h SA treated SFSVs. The curves are vertically shifted for clarity.

whereas the Kiessig fringe periods of all three curves show good agreement for the high-θ region. Individual thickness and roughness values obtained from best-fit simulations to the

Table 1. Individual film thicknesses (Å) of spin-filter spin valve samples obtained from best fits to the experimental XRR data.

	Thickness (Å)		
Layers	As-deposited	6 h UDA	6 h UDA + 38 h SA
NiFeCr/NiFe	29.9	30.1	29.9
PtMn	184.9	183.4	183.2
CoFe	16.4	17.5	17.9
Ru	8.4	7.7	6.6
CoFe/Cu/CoFe/NiFe/Cu	82.7	77.2	79.1
Ta	44.1	47.2	12.5
Ta-oxide	20.5	31.5	90.6

Table 2. Interface roughnesses (Å) of spin-filter spin valve samples obtained from best fits to the experimental XRR data.

	Roughness (Å)		
Layers	As-deposited	6 h UDA	6 h UDA + 38 h SA
NiFeCr/NiFe	2.9	3.1	4.3
PtMn	4.3	3.9	3.2
CoFe	5.0	5.4	5.2
Ru	3.2	3.5	3.5
CoFe/Cu/CoFe/NiFe/Cu	9.3	10.2	8.5
Ta	9.9	10.2	13.3
Ta-oxide	8.3	9.6	10.7

experimental data are summarized in tables 1 and 2. We point out that due to very shallow (electron) density contrast, the interfaces between neighbouring CoFe/Cu/NiFe/CoFe/Cu-oxide layers as well as of NiFeCr/NiFe films are only poorly defined for XRR. Consequently, fitted rms roughness values from these interfaces are affected by relative errors of larger than 100%, and XRR is only sensitive to total thicknesses of these layer sequences and to their outermost interfaces as listed in tables 1 and 2.

The fit results indicate that the UDA and subsequent SA mainly cause a progressive growth of a top tantalum oxide at the expense of the metallic Ta capping layer, as would be expected for a highly reactive metal after heat treatment. An increase of the total film thickness with annealing temperature due to the surface oxidation of the Ta capping layer was also found by Huang *et al* [9]. According to these authors, Ta spontaneously oxidizes to a depth of about 2.5 nm, which is in good agreement with our result for the as-deposited SFSV; see table 1. Whilst there appears to be some growth in the thickness of the tantalum oxide film in TEM micrographs to in excess of 50 Å for the SA treated sample, the TEM results did not indicate such a large thickness as 90 Å. It is nevertheless possible that specimen preparation (especially ion-milling) may have affected the thickness of this outermost layer. All other metallic layer thicknesses listed in table 1 are found to be identical within the error limits of XRR or within the manufacturing tolerances for an SFSV. Furthermore, neither UDA nor SA causes a significant roughness increase—which might be interpreted as the result of an intermixing/interdiffusion process—at any of the interfaces listed in table 2. We note that pure specular XRR cannot distinguish between topographic roughness and interface grading/intermixing to describe the deviation from an ideally flat and smooth interface. For an unambiguous separation of the

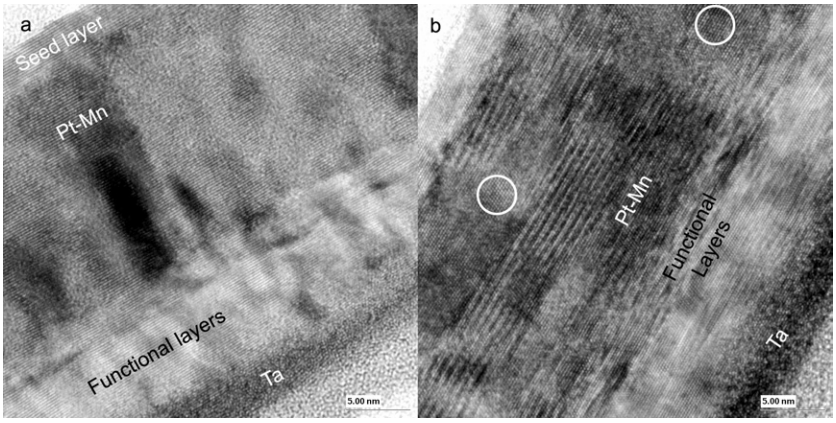

Figure 3. HRTEM images of the as-deposited sensor (a) tilted to display the (111) fringes in all layers with ⟨111⟩ texture from the seed layer up to the final layer before the Ta cap. (b) The fringes parallel to the film plane in the PtMn layer are caused by the overlap of two twin variants in this layer. Representative areas of both twin variants are circled.

two effects additional off-specular scattering curves would have to be recorded and analysed, which is beyond the scope of this paper.

HRTEM was used in order to analyse the influence of UDA and SA treatment on the microstructure of SFSVs. HRTEM images of the multilayer structure in the as-deposited sensor (figure 3(a)) tilted to display the (111) fringes in all layers showed the clear maintenance of the texture from the seed layer up to the final layer before the Ta cap, which is in good agreement with in-plane XRD results (figure 1). A columnar structure appears to be present in the PtMn layer, as expected, and the width of these columns is variable up to at least 40 nm, although it was not possible to attempt any analysis of the grain size based on the limited number of micrographs available. No evidence was found for the presence of any $L1_0$ structure in the PtMn layer in this micrograph or any other of this film. The extensive fringes in the PtMn layer parallel to the film plane in figure 3(b) are in fact Moiré fringes caused by the overlap of two twin variants, both having the (111) texture. Representative areas of both twin variants are circled. In contrast to the XRD results some minor structural disturbance in the first functional layers (CoFe/Ru/CoFe/Cu) is apparent. The Ta appears amorphous, although it could be simply misaligned from any low-index crystal orientation of the nano-crystalline bcc structure displayed in the in-plane XRD patterns (figure 1). It is, however, more likely that it became oxidized to an amorphous oxide in the preparation of the thin TEM sample.

HRTEM images (figures 4(a) and (b)) of the multilayer structure in the 5 h UDA sample display details of the seed layer, the PtMn layer and the top part of the functional layers (figure 4(a)). No significant changes in the NiFeCr and NiFe seed layers can be seen (figure 4(a)) in accordance with the XRR results (tables 1 and 2). A clear (111) texture is still recognizable throughout the multilayer structure. The fct $L1_0$ structure can be clearly recognized in this sample, and a 90° domain boundary between the non-equivalent [110] and [101] orientations of the unit cell is marked with a dotted line in figure 4(a). Figure 4(b) shows the details of the functional layers (CoFe/Ru/CoFe/Cu/CoFe/NiFe/Cu-oxide) and the Ta capping layer. The inner APP functional layers seem to show some structural disturbance in this region, whereas the outer layers appear less affected, if not wholly free of structural disturbances. Nevertheless, a clear (111) texture is apparent throughout these layers. The Ta/TaO_x cap appears mostly amorphous, as for the untreated sample.

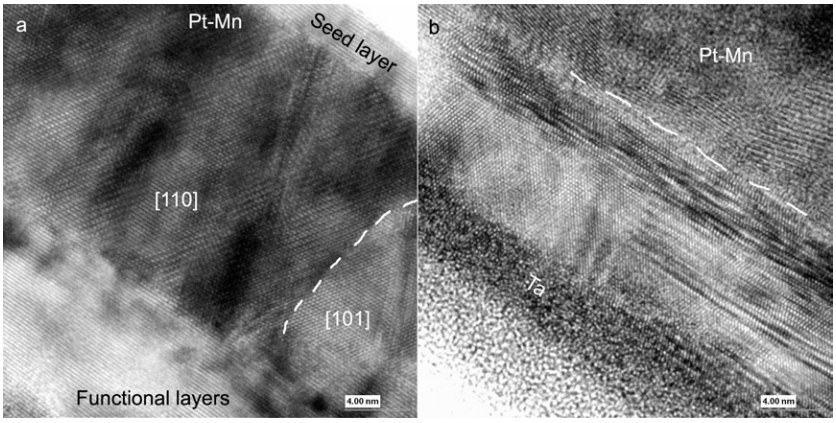

Figure 4. HRTEM images of the sensor after 6 h UDA: (a) details of the seed layer, the Pt–Mn layer and the top part of the functional layers and (b) the details of the functional layers (CoFe/Ru/CoFe/Cu/CoFe/NiFe/Cu-oxide) and the Ta capping layer.

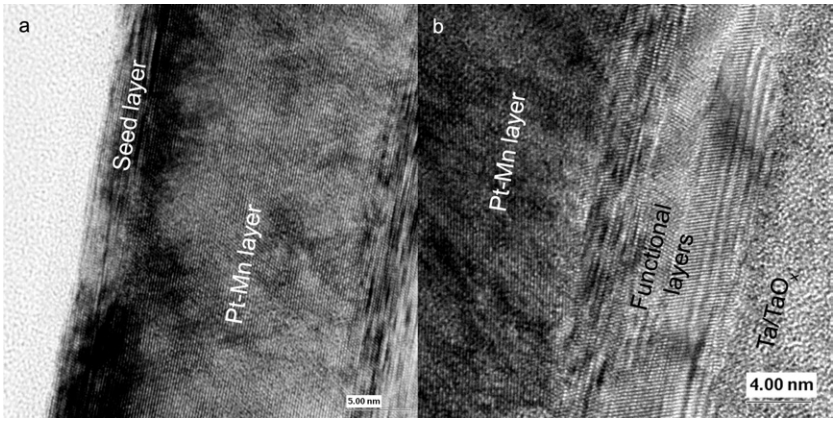

Figure 5. HREM images of the sensor after 6 h UDA + 38 h SA: (a) the seed layer and the PtMn layer and (b) the functional layers and the oxidized Ta capping layer.

HRTEM images of the multilayer structure of the 6 h UDA + 38 h SA sample are shown in figures 5(a) and (b). For clarity the seed layer and the PtMn layer are shown separately in figure 5(a). The seed layer shows some structural disturbance after this heat treatment (figure 5(a)), which is possibly attributable to an intermixing between NiFeCr and NiFe seed layers. This seems nevertheless to have had little effect on the PtMn layer, since this still shows the typical (111) texture (figure 5(a)). The extra annealing also appears to have resulted in a serious disturbance of the functional layers in the form of extensive faulting of both the lower and upper layers, as may be seen in figure 5(b). Moreover, the outer surface appears to show some unevenness, and the Ta cap is hardly visible and has probably been substantially oxidized (figure 5(b)), as expected from the XRR results (tables 1, 2); it was perhaps partially destroyed in sample preparation.

Comparing the HRTEM images taken from as-deposited (figure 3(a)) and 6 h UDA treated (figure 4(a)) SFSV sensors, domain boundaries within large grains caused by the fcc–fct transition during the UDA treatment can be clearly seen in figure 4(a). The GMR and H_{ex}

remains unchanged after 5 h UDA [7]. The increase of the sensor resistance $R(0)$ after 2–6 h UDA reported previously [7] is probably related to this fcc–fct transition in the PtMn layer, possibly with the accompanying disturbance of the APP layers.

The exchange interaction field H_{ex} and GMR performance were found to alter with increasing SA time prior to UDA, but remain unchanged after 12 h SA for the sensors with 5 and 6 h UDA treatments [7]. Some grain growth and defect healing in the PtMn layer may be expected after 38 h SA treatment, which would lead to a reduction of the sensor resistance $R(0)$. However, the $R(0)$ indicated a slight increase with increasing SA time up to 38 h, although the GMR performance and H_{ex} remains unchanged after 12 h SA [7]. This is perhaps attributable to intermixing of the seed layers, and particularly the disturbance of APP and free layers, and possibly also the complete oxidation of the Ta cap layer.

In contrast to the present results, a previous study of top spin valves (SVs) with a Ta/NiFe seed layer and varying PtMn layer thickness revealed that the $R(0)$ and GMR values are constant after 10 h UDA ($T = 270\,^{\circ}$C, magnetic field of 3 kOe), particularly for SVs with a PtMn thickness lower than 20 nm [10]. For these SVs, the alteration of GMR performance and increase of sensor resistance were related to the Mn interdiffusion at the PtMn/CoFe interface [10, 11]. It was reported that the interface of Ta/NiFe seed layers is a major source of interdiffusion after the fcc–fct phase transition in PtMn-based SVs [12]. Compared to other studies on PtMn-based top SVs [10, 12] and on SFSVs [11], in the present study no significant change at the PtMn/CoFe interface was found, suggesting that no significant Mn diffusion across this interface had occurred. Mn diffusion across this interface would reduce the H_{ex}, and the increase of this parameter after SA can be therefore attributed to completion of the fcc–fct transition or defect healing and grain growth in the PtMn layer during the SA treatments. Consequently, we conclude that the SA treatment, i.e. manufacturing conditions resulting in intermixing of NiFeCr/NiFe seed layers, nevertheless does not lead to Mn diffusion. That is to say, Mn diffusion is not the main reason for the alteration of the sensor performance in SFSVs investigated in the present study.

4. Conclusion

The correlation between microstructure and the GMR response as a result of unidirectional annealing and stress annealing treatments of PtMn-based spin-filter spin valves with NiFeCr/NiFe seed layers has been investigated. The fcc–fct transformation in the PtMn layer which is completed after 5–6 h UDA results in the formation of domain boundaries in the PtMn layer and a disturbance of the functional layers. In addition to that, 5–6 h UDA causes a slight oxidation of Ta capping layer. These changes do not influence the GMR performance of the sensor apart from increasing the sensor resistance. Stress annealing for 38 h, which simulates the thermal stability of the finished read-write heads, leads to defect healing in the PtMn layer and an inter-diffusion in the NiFeCr/NiFe seed layers accompanied by more severe structural disturbance of the functional layers and complete oxidation and amorphization of the Ta cap layer. The alteration of the GMR properties up to 12 h SA can be related to these structural changes. In comparison to other studies, intermixing in the seed layer does not affect the PtMn/CoFe interface roughness in the SFSV investigated in this study.

Acknowledgments

RMÖ is indebted to the German Academic Exchange Service (DAAD) for a Research Fellowship and to R Boehmer and F-J Braun, IBM storage technology division, plant Mainz, (Germany) for kindly providing access to deposition tools.

References

[1] Nozieres J P, Jaren S, Zhang Y B, Zeltser A, Pentek K and Speriosu V S 2000 *J. Appl. Phys.* **87** 3920
[2] Saito M, Hasegawa N, Koike F, Seki H and Kuriyama T 1999 *J. Appl. Phys.* **85** 4928
[3] Farrow R F C, Marks R F, Gider S, Marley A C, Parkin S S P and Mauri D 1997 *J. Appl. Phys.* **81** 4986
[4] Anderson G W, Huai Y and Pakala M 2000 *J. Appl. Phys.* **87** 5726
[5] Sato T, Tsunoda M and Takahashi M 2002 *J. Magn. Magn. Mater.* **240** 277
[6] Ladwig P F, Chang Y A, Linville E S, Morrone A, Gao J, Pant B B, Schlutz A E and Mao S 2003 *J. Appl. Phys.* **94** 979
[7] Mustafa Öksüzoglu R, Schug C and York B 2004 *J. Magn. Magn. Mater.* **280** 304
[8] Wormington M, Panaccione C, Matney K and Bowen D K 1998 *Phil. Trans. R. Soc.* A **357** 2827
[9] Huang T C, Nozieres J-P, Speriosu V S, Gurney B A and Lefakis H 1993 *J. Appl. Phys.* **62** 1478
[10] Yang H S, Min K-I, Kim Y K, Lee S R, Park G-S and Song S A 2001 *J. Magn. Magn. Mater.* **226–230** 2070
[11] Anderson G W, Pakala M and Huai Y 2000 *IEEE Trans. Magn.* **36** 2605
[12] Maesaka A, Ishii S and Okabe A 2000 *J. Appl. Phys.* **88** 3982